A Lagrangian analysis of the sources of rainfall over the Horn of Africa Drylands

Akash Koppa[a] , Jessica Keune[a] , Dave A. MacLeod[b] , Michael Singer[c] , Raquel Nieto[d] , Luis Gimeno[d] , Katerina Michaelides[b] , Rafael Rosolem[b] , George Otieno[e] , Abebe Tadege[e] , Diego G. Miralles[a]

[a] *Hydro-Climate Extremes Lab (H-CEL), Ghent University, Ghent, Belgium*

[b] *School of Geographical Sciences, University of Bristol, Bristol, United Kingdom*

[c] *School of Earth and Environmental Sciences, Cardiff University, Cardiff, United Kingdom*

[d] *Centro de Investigación Marinã, Universidade de Vigo, Environmental Physics Laboratory (EPhysLab), Ourense, Spain*

[e] *IGAD Climate Prediction and Application Centre, Nairobi, Kenya*

Corresponding author: Akash Koppa, akash.koppa@ugent.be

ABSTRACT: The Horn of Africa drylands (HAD) are among the most vulnerable regions to hydroclimatic extremes. The two rainfall seasons — long and short rains — exhibit high intraseasonal and interannual variability. Accurately simulating the long and short rains has proven to be a significant challenge for the current generation of weather forecast and climate models, revealing key gaps in our understanding of the drivers of rainfall in the region. In contrast to existing climate modelling and observation-based studies, here we analyze the HAD rainfall from an observationally-constrained Lagrangian perspective. We quantify and map the major oceanic and terrestrial sources of moisture driving the variability in the long and short rains. Specifically, our results show that the Arabian Sea (through its influence on the northeast monsoon circulation) and the southern Indian Ocean (via the Somali low level jet) contribute ~80% of the HAD rainfall. We see that moisture contributions from land sources are very low at the beginning of each season, but supply up to ~20% from the second month onwards, i.e., when the oceanic-origin rainfall has already increased water availability over land. Further, our findings suggest that the interannual variability in the long and short rains is driven by changes in circulation patterns and regional thermodynamic processes rather than changes in ocean evaporation. Our results can be used to better evaluate, and potentially improve, numerical weather prediction and climate models, which has important implications for (sub)seasonal forecasts and long-term projections of the HAD rainfall.

1. Introduction

Rainfall in the Horn of Africa drylands (HAD) — the semi-arid and arid parts of Somalia, Ethiopia, and Kenya (Figure 1a) — is crucial for sustaining the region's predominantly rainfed agriculture and pasture-dependent livelihoods. This reliance of livelihoods on rainfall renders the region highly vulnerable to hydroclimatic extremes (particularly droughts), which frequently cascade into high levels of food insecurity and humanitarian crises, especially when compounded with social conflict and high vulnerability. The vulnerability of the HAD region has recently been evidenced by the severe impacts caused by the successive failure of the two main rainfall seasons — long (March–May, MAM) and short (October–December, OND) rains — since 2020 (FEWSNET 2022). Likewise, an anomalously strong Indian Ocean Dipole (IOD) (Saji et al. 1999), resulting in enhanced moisture transport from the Indian Ocean, has also caused major floods during the short rains in recent years, such as the unprecedented flooding in 2019 (Nicholson et al. 2022). Furthermore, shifts in the frequency and intensity of climate extremes due to climate change are expected to exacerbate flooding, food insecurity (Brown and Funk 2008), and human conflicts (Hsiang et al. 2013; Maystadt and Ecker 2014). Projections of drought, on the other hand, remain highly uncertain in the region, with strong divergence among models (Haile et al. 2020). In this regard, it is imperative that our current understanding of the drivers and predictability of rainfall in the HAD region is improved, which can bring novel insights and opportunities for model benchmarking. Then, if accurate and timely rainfall forecasts were available, that would help enhance preparedness and design adequate adaptation and mitigation measures.

While the interannual variability of the short rains is strongly associated with coupled ocean–atmosphere oscillations — specifically the El Niño Southern Oscillation (ENSO) and the IOD (Behera et al. 2005; Manatsa and Behera 2013; Nicholson 2015; MacLeod et al. 2021) — the drivers of the long rains are more complex and have been the subject of much debate. In the past four decades, the long rain season in the HAD region has exhibited a consistent drying trend, contrary to projections from global climate models, a phenomenon termed as the *East African Climate Paradox* (Rowell et al. 2015; Tierney et al. 2015; Wainwright et al. 2019). Both ocean–atmospheric teleconnections and local phenomena have been posited as plausible causes for this observed drying trend. For example, the suppression of convection over Eastern Africa is strongly linked to the warming of the tropical western Pacific Ocean and the Indian Ocean (Williams and

Funk 2011). Additionally, zonal gradients in sea surface temperatures between Indonesia and the Central Pacific have been postulated as a significant driver (Liebmann et al. 2014). Funk et al. (2018) also highlighted the association of a fast-warming region in the west Pacific Ocean, termed as *Western V*, with the frequency of droughts during the long rain season, and its recent long-term drying. Meanwhile, an evaluation of instrumental and reanalysis datasets by Vellinga and Milton (2018) suggested that the most significant factors influencing long rains variability are: the Madden-Julian Oscillation (MJO), sea surface temperatures in the north-west Indian Ocean, and the Quasi-Biennial Oscillation. Combined, these three factors can explain up to 25% of the interannual variance in precipitation. Likewise, around 18% of the decadal drying trend in the long rains has been attributed to the variability of the MJO (Walker et al. 2020). The importance of the north-west Indian Ocean is supported by climate model experiments (MacLeod 2019), which point to near-surface processes in the north-west Indian Ocean as a key control on long rains, particularly though changes in air humidity. MacLeod (2019) also demonstrated that the south-west Indian Ocean emerges as a dominant control on May rainfall, highlighting the influential role of Somali jet variability. This strong intraseasonal variability was also highlighted by Dyer and Washington (2021) who diagnosed heterogeneous processes occurring throughout the season after dividing the three months into four discrete periods.

To date, most studies on the long and short rain seasons in the HAD region have focused on identifying relevant ocean–atmospheric teleconnections. However, very few studies have analyzed the origins of HAD rainfall in terms of moisture sources and their variability (Nieto et al. 2014). Insight into moisture sources can be provided with Lagrangian atmospheric transport models, which are widely used to identify the local and external sources of moisture contributing to rainfall over specific regions (Stohl et al. 2005; Sodemann et al. 2008; Keune et al. 2022). These models have highlighted, for instance, the critical importance of land evaporation in sustaining rainfall over different river basins around the world (Drumond et al. 2008; Sorí et al. 2018; Fremme and Sodemann 2019; Keune and Miralles 2019). Other studies have quantified the primary sources of extreme rainfall over distinct hydroclimatic regions such as Nepal (Bohlinger et al. 2017) and the Mediterranean (Insua-Costa et al. 2022). Lagrangian models have also been useful in understanding not only the role of moisture transport in exacerbating droughts (Herrera-Estrada et al. 2019; García-Herrera et al. 2019; Holgate et al. 2020), but also their downwind impacts, which enhances spatial

drought propagation (Schumacher et al. 2022), heatwave aggravation (Schumacher et al. 2019), and a cascading of ecological impacts (Zemp et al. 2017). Several studies have traced the origin of rainfall occurring over various regions in sub-Saharan Africa. For example, local evaporation was found to be an essential source of moisture for rainfall over the western Sahel (Nieto et al. 2006). Local moisture recycling has also been shown to sustain the Congo rainforest (Dyer et al. 2017), potentially leading to its expansion in the future (Staal et al. 2020). Salih et al. (2015) used Lagrangian models to identify Central Africa and the Arabian Peninsula as the regions with the largest contribution to the Sahelian-Sudan summer rainfall. Lagrangian models have also proved useful to unravel pathways by which moisture is transported to the West African Monsoon system (Niang et al. 2020). Despite the existence of these studies for other sub-Saharan regions, little is documented about the moisture source regions of rainfall over HAD, and the relative importance of land and oceanic moisture contributions to the trends in the long and short rains in the region.

In this study, we aim to close this research gap through the application of a Lagrangian atmospheric transport model to identify the source regions which contribute moisture during the two HAD rainfall seasons. Specifically, we seek to quantify the relative importance of oceanic and terrestrial sources of moisture for the long and short rains during normal and extreme seasons. Then, for each rainfall season, we illustrate the differences in the source regions between anomalously wet and dry years, and study the possible upwind causes explaining the changes in the moisture supply for rainfall. This study represents a step towards improving our understanding of the drivers of the recent and future interannual changes in the long and short rains using Lagrangian analysis. Furthermore, accurately delineating the source regions of moisture can aid in more efficient selection of rainfall predictors for seasonal forecasting, and thus may potentially enable more accurate forecasts in the region (Deman et al. 2022).

2. Methods and Data

a. Quantification of Rainfall Moisture Sources

Lagrangian identification and quantification of the source region of rainfall over a specific 'sink' region (HAD in this case) consists of two main phases. In the first phase, the output of a Lagrangian atmospheric transport model is used to track air parcels over the HAD backward in time, i.e., from the sink to the source regions. In the next phase, the Lagrangian trajectories are evaluated by

using different meteorological criteria to track the changes in moisture of the air parcels as they travel from the source regions to the sink region. In this section, we first describe the Lagrangian atmospheric transport model used in the study and then detail the moisture tracking framework used to evaluate the air parcels.

1) Lagrangian Model Simulations

The Lagrangian transport model used in this study is the Flexible Particle Dispersion model (FLEXPART) version 9.01 (Stohl et al. 2005) driven with reanalysis data (Dee et al. 2011). The model simulations are carried out at a global scale using approximately two million air parcels which are uniformly distributed throughout the globe and are tracked both in space and time. The following variables are used to force FLEXPART: temperature, specific humidity, horizontal and vertical wind, cloud cover, precipitation, 2-m air temperature, dew-point temperature, sensible and latent heat fluxes, and North/South and West/East surface stress. FLEXPART tracks the location (latitude, longitude, and height) of each of the two million parcels and simulates their dynamic and thermodynamic properties (temperature, density, specific humidity). Using ERA-Interim data as forcing (see below), these outputs are available at 3-hourly timesteps, but we only use 6-hourly reanaylses for the evaluation.

2) Identification and Quantification of Rainfall Moisture Sources

Outputs from FLEXPART are used to construct and evaluate the trajectories of air parcels, i.e., all air parcels residing over the HAD region are tracked backward in time and parsed for precipitation in the sink (HAD) region to identify moisture sources in previous time steps and locations. In doing so, all the locations in which the air parcel gains or loses moisture are traced. In this study, the analysis of air parcel trajectories from the FLEXPART simulations are carried out using a recently developed moisture tracking framework (Keune et al. 2022). Within the framework, the trajectories are evaluated using a three-step process consisting of diagnosis, attribution, and bias-correction, as described below.

In the diagnosis step, a dataset of process (rainfall and evaporation) detection is generated by evaluating *all* global two-step trajectories. Thus, for every air parcel and every time step in the global FLEXPART simulations, precipitation (P) and evaporation (E) are detected from changes in specific humidity based on the following mass balance:

$$e - p = m * \Delta q \tag{1}$$

where, e and p (both in kg) represent net gains and losses in specific humidity for each parcel from evaporation and precipitation, respectively. m is the mass of the parcel (kg). Δq is the change in specific humidity ($kg.kg^{-1}$) of the parcel between two consecutive time steps along a parcel's trajectory. A parcel is assumed to contribute to a rainfall event if it undergoes a net loss of specific humidity between consecutive time steps ($\Delta q < 0$) and the mean relative humidity (RH) is higher than 80% (Sodemann et al. 2008), following the convection parameterization by Emanuel (1991). Then, rainfall over a specific area (A) can be estimated by integrating over individual contributions of all the air parcels n as

$$P = \frac{1}{A} \sum_{i}^{n} \Delta q_i (\Delta q_i < 0 kg.kg^{-1}, RH_i > 80\%) \tag{2}$$

Similarly, E is identified if the air parcel experiences a net gain of specific humidity between two consecutive time steps ($\Delta q > 0$) and the parcel resides within the atmospheric boundary layer (ABL). Integrating contributions from every air parcel, E over an area (A) is estimated as:

$$E = \frac{1}{A} \sum_{i}^{n} \Delta q_i (\Delta q_i > 0 kg.kg^{-1}, z_i < h_{ABL}^{max}) \tag{3}$$

where, z_i is the height of the parcel (m) and h_{ABL}^{max} is the maximum height of the ABL between the two time steps considered. Finally, the accuracy and reliability of the P and E detection is evaluated using multiple criteria (details in Keune et al. (2022)).

In the attribution step, the detection criteria ($RH_i > 80\%$ and h_{ABL}^{max}) detailed above are used to evaluate the air parcels that reside over the HAD region (Figure 1). Specifically, every parcel within the HAD region which satisfies the P detection criteria, indicating rainfall, is tracked back in time for a maximum of 15 days, which includes the long tail of the distribution of the residence time of atmospheric water vapor (Sodemann 2020). All moisture gains and losses experienced by the parcel along its trajectory are identified. Then, a quantitative attribution of evaporation in the source region to rainfall in the sink region (HAD in this case) is carried out. This is a non-trivial task as the moisture uptake experienced by the air parcel can be lost as rain *en route* to the sink

region, and rain events have to be discounted using objective criteria. Here, we adopt the method of linear discounting proposed by Sodemann et al. (2008) which assumes that the air is well-mixed at all times. Therefore, it is assumed that the moisture lost at a particular time step ($t = i$) in the parcel trajectory has originated from moisture taken up in previous time steps ($t < i$), and the contribution of moisture uptake to the rainfall at time step $t = i$ is proportional to the magnitude of moisture uptakes in the previous time steps. Using this method, the fractional contribution of each source region to the sink region rainfall is calculated by discounting all *en route* losses. This procedure allows us to establish a mass-conserving source–sink relationship that describes the contribution of surface evaporation in the source region to precipitation in the sink.

Finally, biases arising from uncertainties in P and E detection criteria are corrected using the accuracy information estimated in the diagnosis step with observations of evaporation and precipitation in the source and sink regions, respectively. First, evaporation from the source region is bias-corrected using the unconditional E flux calculated using all the air parcels over the source region (from the diagnosis step) and satellite-based E. Then, the sink region rainfall over HAD is bias-corrected using observational estimates and the contributions from the different source regions are proportionally scaled. The bias-corrections are carried out on a daily timescale.

b. Reanalysis and Satellite-based Datasets

Various hydroclimatic variables from both reanalysis and satellite-based datasets are used to drive the FLEXPART Lagrangian model and bias-correct its outputs. The model is forced with ERA-Interim global reanalyses (Dee et al. 2011) at 1° spatial resolution. Variables at single and multiple model levels (60-levels) extending from the surface towards the top of the atmosphere are used. The data spans the entire globe, and is available at 1.0° spatial resolution. Here, the six-hourly reanalysis product and the respective three-hourly reforecasts are used for a time period of 37 years (1980–2016). The choice of ERA-Interim is motivated by the requirement of multiple consistent meteorological variables, as described above. For the bias-correction of precipitation, we use the Multi-Source Weighted Ensemble Precipitation, version 2 (MSWEP v2.8) dataset (Beck et al. 2019). The MSWEP dataset, spanning a time period of 1979–present, is generated by merging the Integrated Multi-Satellite Retrievals for the Global Precipitation Measurement (IMERG) data (Huffman et al. 2015) and the ERA5 reanalysis product (Hersbach et al. 2020) using *in situ*

observations, and it is available at a spatial resolution of 0.1° and a 3-hourly timestep. MSWEP v2.8 was selected as it shows considerable skill over East Africa (e.g. Sahlu et al. (2017))To bias-correct evaporation, terrestrial evaporation from the Global Land Evaporation Amsterdam Model (GLEAM) version 3.5a is used (Miralles et al. 2011; Martens et al. 2017). This dataset is available at 0.25° at daily temporal resolution, spanning the years of 1980–2020. For ocean evaporation, we use the Objectively Analysed Air-Sea Fluxes (OAFlux) dataset (Yu and Weller 2007). The spatial and temporal resolution of OAFlux is 1° and daily, respectively, and is available for the years 1958–2019.

c. Change Point Detection

We employ the Pettitt test (Pettitt 1979) to analyze whether the rainfall regime during the long and short rains has undergone an abrupt change over the study period (1980–2016) in the HAD region. The Pettitt test is a non-parametric approach to detect significant changes in the statistical behavior of a time series. The time step at which the behavior significantly changes is identified as the *change point*. Formally, one may consider a time series of random variables $Y_{t=1}, Y_{t=2}, \ldots Y_{t=T}$; according to the Pettitt test, the time series is said to have a change point at time $t = \tau$ if $Y_{t=1} \ldots Y_{t=\tau}$ have a common distribution function F_1 and $Y_{t=\tau} \ldots Y_{t=T}$ have a different distribution function F_2. The Pettitt test does not make a priori assumptions about the functional forms of F_1 and F_2. For a detailed mathematical description of the Pettitt test, we refer the readers to Rybski and Neumann (2011). In this study, the *pyhomogeneity* Python package was used to implement the test. The exceptional ENSO year 1997 has been removed from the change point analysis of the short rains.

3. Results

a. Climatology of Rainfall

Over the study region, the long rain season accounts for ~50% of the annual rainfall while the short rains account for ~38% (Figure 1b). The HAD region has witnessed considerable interannual variability in both seasons, as observed in the 37 years of the MSWEP v2.8 data (Figure 1c and d). A change point detection analysis reveals the existence of distinct change points for the long rains in 1998, and for the short rains in 2001. The anomalously dry long rains post-1998 reported by other studies are distinctly visible in the study region, while some recovery is seen in the later

years, although subjected to high interannual variability. These are results are in agreement with recent studies which identified distinct wet (1980–1997), dry (1999–2011), and recovery (from 2012 onwards) periods (Wainwright et al. 2019; Walker et al. 2020). The mean reduction in the long rains after the change point is ~45 mm, i.e., a decrease of ~26% compared to the mean rainfall over 1980–1997). In contrast to the long rains, the short rains become more abundant after the 2001 change point, albeit to a smaller extent. The mean increase in rainfall between the dry (1980–2000) and wet (2002–2016) periods is ~36 mm, i.e., an increase of ~40% compared to the mean over the previous years. From 1998–2012, all the months during the long rains are dry, except for April in 2002 and 2006. Similarly, the anomalies in short rains are driven by uniform increases and decreases in rainfall during all its constituent months, with few exceptions. We clearly see the impact of the unprecedented El Niño event in 1997 (McPhaden 1999) on all the three months of the short rains, and to a lesser extent in 2006 and 2015 (which have been documented as years of high groundwater recharge (Adloff et al. 2022)), and during the exceptional drought of 2010.

b. Climatology of Source Regions

The climatological moisture source regions for the long and short rains are presented in Figure 2. To better understand the role of circulation patterns in influencing rainfall over the region, long-term mean integrated water vapour transport (IVT) maps for the two seasons are plotted (Figure 2) using ERA-Interim data. During the long rains, the role of the Indian Ocean as the predominant moisture source to the HAD region is evident (Figure 2a). The source region consists of two distinct lobes in the Indian Ocean, one in the Northern Hemisphere (hereafter referred to as 'NIO') and one in the Southern Hemisphere (hereafter referred to as 'SIO'). While the NIO lobe stretches to the Arabian Sea on the western coast of the Indian peninsula, the SIO lobe encompasses a much larger area. The NIO and SIO lobes converge close to the HAD region. Although the source region spans a large area, half the rainfall during the long rains is estimated to originate from oceanic regions in close proximity to the HAD (red contour in Figure 2a). From the mean IVT map for the long rains (Figure 2c), it is evident that the SIO region, the largest source moisture for HAD rainfall, is part of a large band of moisture which stretches across the tropics. We see that much of the moisture is transported to the southern parts of the HAD. The air above the NIO is relatively dry, which coincides with the existence of a persistent anticyclonic circulation pattern in the Arabian Sea 2c).

Additionally, we track the spatial dynamics of the long rains source regions and the corresponding wind patterns for the months of March, April, and May (Figure 3a, b, and c). We see that the moisture for the long rains is initially sourced from evaporation in the NIO in March. From the wind circulation patterns, it is clear that the lack of moisture contribution from the SIO coincides with the lack of winds from the region. As the long rain season progresses, the regions of the most intense moisture contributions gradually shift to the SIO during April and May (Figure 3b and c). As the contribution of March rainfall to the total rainfall is the lowest among the three months (Figure 1b), moisture from the SIO forms the major source during the long rains (Figure 2a). This agrees with the IVT results presented in Figure 2c and shows the importance of both moisture availability and circulation in affecting the moisture contribution to rainfall during the long rain season.

The source region of rainfall during the short rains has a spatial pattern similar to that of the long rains, with two distinct lobes in the Northern and Southern Hemispheres (Figure 2b), and a relatively small proximate region contributing 50% of the rainfall (red contour in Figure 2b). Although the total rainfall during the short rains is less than during the long rains, the extent of the source region is larger, with the NIO lobe reaching as far as the Indian subcontinent. The change in the wind circulation patterns between the long and short rains is evident (Figure 2d), with the consequence being higher moisture transport from the NIO region. Temporally, the progression of the source regions through the months of October, November, and December is similar to that of the long rains, with the main difference being that the rains are initiated by moisture transport from the SIO lobe rather than the NIO region (compare Figure 3d with Figure 3a). In the subsequent months (November and December), the regions contributing the largest amount of evaporation are in the Northern Hemisphere (Figure 3e and f). Unlike the long rains, the NIO and SIO are equally important as source regions for rainfall. Finally, as for the long rains, higher moisture contributions from the NIO and SIO are generally associated with favourable circulation conditions and stronger winds.

To quantify the relative importance of different regions for rainfall over the HAD, we differentiate between three distinct source regions: a) *local land*, i.e. any land areas within the HAD region, b) *ocean*, and c) *external land*, i.e. any land areas outside the HAD region. The contribution from local land evaporation to HAD precipitation is defined the *local recycling*. Table 1 shows

the percentage of total rainfall that originates from each of the three regions. The dominant role of the ocean as a source of moisture for rainfall during the long and short rains is reflected in the relative contributions, in which evaporation from the oceans contributes more than 75% of the total moisture. In terms of local land contributions, local recycling of moisture plays a greater role during the short rains compared to the long rains. Decomposing the relative contributions into the constituent months, we see that the land contributions (both external and local recycling) are the lowest during the first month of both seasons (March for the long rains and October for the short rains). The land contributions peak during the second month of both seasons, with as much as 28% of the short rains coming from land evaporation (local recycling plus external land contributions) in November (see Table 1).

TABLE 1. Percentage contribution and associated standard deviation of different source regions to rainfall over the HAD region calculated for the time period 1980–2016.

Source	Long Rains	Short Rains	March	April	May	October	November	December
Local Recycling	10.9 ± 3.1	13.8 ± 4.3	7.1 ± 5.4	15.0 ± 4.9	10.7 ± 3.0	11.9 ± 3.9	17.3 ± 5.2	12.2 ± 6.3
Ocean	78.6 ± 5.0	76.7 ± 5.3	84.5 ± 8.2	73.4 ± 7.3	77.9 ± 5.9	80.7 ± 5.4	72.0 ± 6.1	77.6 ± 7.5
External Land	10.5 ± 2.3	7.6 ± 1.3	8.4 ± 4.2	11.6 ± 2.9	11.4 ± 3.8	7.4 ± 1.9	10.7 ± 1.5	10.2 ± 2.2

c. Trends and Multi-annual Variability in Sources

While the previous section focused on quantifying the climatological mean source regions of both the long and short rains, here we quantify the temporal changes in the moisture contributions of the three source regions (defined above) to the total rainfall during both seasons. This is especially important given the large year-to-year variability in rainfall that impacts the HAD region (Adloff et al. 2022). Further, we identify the regions from which moisture contribution is enhanced/inhibited during anomalously wet and dry years. From Figure 4a, we see that the moisture contributions from all the three source regions are closely correlated with total rainfall: both land and ocean contributions concurrently increase or decrease with total rainfall. A few exceptions exist (years 1983, 1998, 2002, 2003, and 2005), wherein land contributions were anomalously negative while ocean contributions were positive (note that anomalies are not shown in the figure).

To quantify this apparent association among the three sources, we estimate the pairwise correlation among them. We see that the two land sources (local and external land) have the highest correlation (0.94), followed by ocean contributions and local recycling (0.84), and, finally, ocean contributions and external land (0.79). Further, we estimate the difference in relative moisture contributions from the three sources before and after the change point in 1998. The absolute moisture contribution from the oceans, the largest (Table 1), has witnessed a reduction of ~25% (-33.8 mm) compared to the pre-change point period; while the relative importance of oceanic moisture remains similar. Simultaneously, locally recycled moisture has decreased by ~33% (-6.8 mm) and from 12 to 10% after 1998. Finally, the moisture contributions from external land surfaces experienced a change of ~-23% (-4.3 mm).

Similar to the long rains, we see that the moisture contributions from each of the source regions during the short rains are strongly correlated with each other (Figure 4b). We do not see any year in which land sources have alleviated moisture deficits from the ocean, i.e., anomalously enhanced or inhibited moisture contribution from the ocean is also associated with enhanced or inhibited moisture contribution from the land (Figure 4b). Next, we analyze the changing moisture contribution from the different sources before and after the change point in 2001. While the absolute ocean contribution has seen an increase of ~31% (21.6 mm) along with an increase of the total rainfall after the break point, the relative importance of ocean evaporation for rainfall during the short rains has been decreasing (from 78 to 75%). Meanwhile, the land contributions have witnessed a remarkable change with the locally recycled moisture and external land contributions increasing by ~80% (9.7 mm) and ~59% (4.9 mm), and in relative terms from representing 13 to 15% and 9 to 10% of the total rainfall, respectively.

d. Source Regions During Dry and Wet Years

To better understand the variability of the source regions during extreme rainfall, we first average the source regions of the five wettest (1981, 1985, 1987, 1988, 1990) and driest (1999, 2004, 2008, 2009, 2011) years of the long rains (Figure 5a and b). The spatial extent of moisture-contributing regions is similar between wet and dry years, with the main difference being the absolute magnitude of the moisture contribution from the source regions. To better understand the magnitude by which moisture contribution to rainfall is enhanced or inhibited in the source regions, we calculate the

anomalies of source region contributions for the wet and dry years (Figure 5c and d). The higher rainfall during the wet years can be attributed to enhanced moisture contributions from relatively small areas in close proximity to the HAD region. In fact, the contribution from a substantial part of the *SIO* is anomalously low. In contrast, the reduced rainfall in dry years is a result of severely inhibited moisture contribution from most of the source region, with only a small area in the *SIO* exhibiting near-zero or positive anomalies. Interestingly, the difference in wind speed between wet and dry years is negligible.

We perform a similar analysis for the short rains by averaging the source regions of five wettest (1982, 2004, 2006, 2011, and 2015) and driest (1983, 1991, 1998, 2005, and 2010) years (Figure 6a and b), respectively, and estimate their anomalies (Figure 6d and e). The wet years are typically associated with positive ENSO and IOD; the seasonal mean of the multivariate ENSO index ((https://www.psl.noaa.gov/enso/mei/) and the Dipole Mode Index (https://psl.noaa.gov/gcos_wgsp/Timeseries/DMI/) over the 5 years were +1.1 and +0.35 respectively. The dry-year seasonal mean of the multivariate ENSO index and the Dipole Mode Index were -0.64 and -0.18 respectively. Unlike the long rains, we see a tangible increase in the area of the source regions contributing moisture during the wet years compared to the dry years (compare Figure 6a and b), with even land areas in the Indian subcontinent contributing meaningfully to rainfall. In addition, moisture contributions from most of the source regions are anomalously positive (Figure 6d), in contrast to the long rains in which enhanced moisture contributions were only seen from regions proximate to the HAD (Figure 5c). Similarly, the anomalies for the dry years indicate that moisture contribution is inhibited from the entire source region. As the short rains are closely associated with ENSO and IOD (MacLeod et al. 2021), the expansion and contraction of the source regions is likely related to the strength of these oscillations.

An extreme case of the ENSO and IOD influence is seen in 1997 McPhaden (1999). The multivariate ENSO index was at an unprecedented value of +2.0 and the Dipole Mode index was recorded at a historically high value of +1.2. We see that the record high rainfall of approximately 300 mm averaged over the HAD region originated from a much larger source region than normal (Figure 6c), with an expansion of both *NIO* and *SIO* lobes. Additionally, anomalies of ocean moisture contribution were exceedingly positive over the entire source region, with magnitudes doubling that of even the other wet years (compare Figure 6d and f). Similar to the long rains,

we observe no significant changes in either the average wind direction or associated circulation patterns across the wet, dry, or ENSO-dominated years. However, we do notice stronger westerlies across the equatorial Indian Ocean. On the contrary, wind speeds are marginally higher during the dry years, despite the lower moisture contributions.

4. Discussion

a. Indian Ocean as the Dominant Source of Moisture for HAD Rainfall

The results of this study re-emphasize the dominant role of the Indian Ocean as a moisture source for the long and short rains in the HAD region (Williams and Funk 2011; Funk et al. 2016; Wainwright et al. 2019; Walker et al. 2020). In fact, on a global average, oceanic moisture sources are likely becoming more important for continental rainfall as a result of climate change (Findell et al. 2019; Gimeno et al. 2020). Therefore, a key step in improving the current understanding of the intraseasonal and interannual variability of the two rain seasons in HAD is to accurately characterize the variability in moisture source regions within the Indian Ocean. In this regard, our results agree with previous global-scale studies; based on ERA-Interim reanalysis as well, van der Ent and Savenije (2013) and Nieto et al. (2014) delineated source regions of continental precipitation that agree with the NIO and SIO lobes in Figure 2. These two regions are among the fifteen major oceanic sources of terrestrial rainfall identified by van der Ent and Savenije (2013), and similar sources were also portrayed by Gimeno et al. (2010). Further, the evolution of the predominant source regions – from (a) NIO to the SIO through the months of March, April, May during the long rains and (b) from SIO to the NIO over the course of the three months (OND) during the short rains — seen in Figure 3 — matches the findings of van der Ent and Savenije (2013) and MacLeod (2019). The NIO region (2) is consistent with the circulation patterns associated with the north-east monsoon during which moisture-laden winds blow from the Western Ghats mountain range in India towards Somalia (November, December, and March in Figure 3) (Funk et al. 2016). On the other hand, the SIO moisture source region encompasses regions influenced by the Somali low-level jet, a well known conveyor of moisture to East Africa during the months of April, May, and October (Figure 3) (Munday et al. 2021).

Figures 5 and 6 show that variability in rainfall over the HAD region is strongly driven by the near-uniform inhibition/enhancement of moisture contribution from all oceanic source regions.

However, delineating source regions and their moisture contributions alone is insufficient to fully understand the primary reasons for changes in moisture contributions. To address this, we compare the precipitation over the HAD region with the total evaporation (as opposed to moisture contributions to rainfall) from the source regions for the long and short rains (Figure 7). From Figure 7, it is clear that long rain precipitation and evaporation in the source region are, in fact, anti-correlated (correlation coefficient of -0.52). Similarly, the short rains exhibit negative correlation with source region evaporation, albeit with a lower correlation coefficient of -0.15. This indicates that changes in the long and short rains are not primarily controlled by changes in ocean evaporation in source regions. From this we infer that rainfall changes must be driven instead by atmospheric circulation and dynamic and thermodynamic processes determining atmospheric stability in the sink region.

b. The Importance of Terrestrial Evaporation for HAD Rainfall

While the contribution of terrestrial moisture sources to rainfall in the HAD region is low, it is nevertheless still substantial, with 20–25% of the rainfall originating over land. In an arid region like the HAD, land contributions can be the difference between a drought and an average rainfall season (Miralles et al. 2016). However, this does not imply that the land contributions can alleviate the reduced moisture contribution from oceans during the dry years. As evident from our results, ocean and land contributions are closely correlated with each other. During the long rains, the contribution from land generally increases if contributions from the ocean to rainfall over HAD increase too (the correlation between ocean contributions and locally recycled moisture is 0.84; external land and ocean contributions exhibit a correlation of 0.79). This may partly be due to the fact that the dry season water availability over land in the HAD is very low (Figure 1b) and thus most of the water available for evaporation, and the subsequent recycling, is dependent on the quantity of rainfall during the first month of the long rain season. This hypothesis is supported by increased local contributions during the second month of the rain season. Similarly, during the short rains, the correlations between ocean contribution and locally recycled and external land contributions are 0.93 and 0.98 respectively. There exists a strong association of the short rains with large scale ocean–atmosphere oscillations such as ENSO and IOD, during which land evaporation is dependent on the quantity of rainfall in the first month of the short rains (October).

We contextualize the importance of land contributions in the HAD region by comparing them with different regions across Africa. In contrast to the dominant role of the Indian Ocean reported above, the Sahel region in Sudan derives the majority of its moisture (~60%) from terrestrial sources (Salih et al. 2015). Similarly, land-derived moisture contributions account for ~60% and ~44% of the rainfall over the Congo rainforest (Tuinenburg et al. 2020) and West Africa (Gong and Eltahir 1996) respectively. Continental scale studies have shown that ~50% of the rainfall over Africa is derived from terrestrial sources (van der Ent et al. 2010; Te Wierik et al. 2022). However, there exist some spatial variability; for example, in the Limpopo river basin in southern Africa (Rapolaki et al. 2020) which is closer to the oceans compared to the Sahel, the moisture sources are predominantly oceanic. However, proximity to the oceans does not necessarily imply greater moisture contribution from them (for example the Yangtze River valley in Asia (Fremme and Sodemann 2019)). The local recycling results reported in this study (Table 1) are in line with a global analysis of water-limited regions which showed that local recycling can contribute 3%–35% of the rainfall in dry regions (Miralles et al. 2016).

5. Conclusion

The delineation of the source regions of rainfall for the HAD, and the quantification of the relative contributions of ocean and land, are key steps in deriving new insights into the drivers of the HAD rainfall at multiple timescales. In this regard, this study mapped the main sources of moisture associated with the north-east monsoon and the Somali low level jet, the two main atmospheric circulation patterns which transport moisture to the HAD region. Our results reveal that while land contributions are becoming increasingly important for the short rains in the recent years, the importance of ocean contributions is increasing for the long rains. At seasonal and subseasonal scales, the source regions derived with the Lagrangian analysis have the potential to improve the predictability of the long and short rains through both better selection of predictors (Deman et al. 2022) and improving the understanding of their drivers. Therefore, our results can be used to augment drought and flood early warning systems, which are important tools in the region to prepare appropriate mitigation measures (Funk et al. 2019). The relatively small but substantial moisture contribution from land during the two rain seasons highlights the importance of vegetation transpiration, interception loss, and soil evaporation as sources of rainfall. At

interannual timescales, the Lagrangian perspective provided in this study can help disentangle the complex drivers of the two rain seasons, especially the more elusive drivers of the long rains. In this regard, our results highlight the complex combination of drivers (changes in source region evaporation, regional circulation patterns, and local atmospheric stability) that potentially drive the variability in long rains. Specifically, we find that during the long rains evaporation from the source region is anti-correlated with rainfall in the HAD. Unravelling the mechanisms behind this strong anti-correlation can provide insights into drying of the long rains and thus the *East African paradox*. At decadal time scales, the source regions enable novel ways of evaluating the current generation of climate models, which still exhibit a high degree of uncertainty and disagreement in simulating rainfall over the region.

Acknowledgments. The study was funded by the European Union Horizon 2020 Programme (DOWN2EARTH, 869550). The computational resources and services used in this work were provided by the VSC (Flemish Supercomputer Center), funded by the Research Foundation, Flanders (FWO), and the Flemish Government.

Author contributions. A.K., J.K., and D.G.M conceived the study and designed the experiments. A.K. conducted the analysis with inputs from J.K., D.A.M., and D.G.M. A.K. wrote the paper with contributions from all coauthors. All coauthors contributed to the interpretation and discussion of results.

Data availability statement. The raw data supporting the conclusions of this article will be made available by the authors, without undue reservation.

References

Adloff, M., M. B. Singer, D. A. MacLeod, K. Michaelides, N. Mehrnegar, E. Hansford, C. Funk, and D. Mitchell, 2022: Sustained water storage in horn of africa drylands dominated by seasonal rainfall extremes. *Geophysical Research Letters*, **49 (21)**, e2022GL099 299, doi:https://doi.org/10.1029/2022GL099299, URL https://agupubs.onlinelibrary.wiley.com/doi/abs/10.1029/2022GL099299, e2022GL099299 2022GL099299, https://agupubs.onlinelibrary.wiley.com/doi/pdf/10.1029/2022GL099299.

Beck, H. E., E. F. Wood, M. Pan, C. K. Fisher, D. G. Miralles, A. I. J. M. van Dijk, T. R. McVicar, and R. F. Adler, 2019: Mswep v2 global 3-hourly 0.1° precipitation: Methodology and quantitative assessment. *Bulletin of the American Meteorological Society*, **100 (3)**, 473 – 500, doi:10.1175/BAMS-D-17-0138.1, URL https://journals.ametsoc.org/view/journals/bams/100/3/bams-d-17-0138.1.xml.

Behera, S. K., J.-J. Luo, S. Masson, P. Delecluse, S. Gualdi, A. Navarra, and T. Yamagata, 2005: Paramount impact of the indian ocean dipole on the east african short rains: A cgcm study. *Journal of Climate*, **18 (21)**, 4514 – 4530, doi:10.1175/JCLI3541.1, URL https://journals.ametsoc.org/view/journals/clim/18/21/jcli3541.1.xml.

Bohlinger, P., A. Sorteberg, and H. Sodemann, 2017: Synoptic conditions and moisture sources actuating extreme precipitation in nepal. *Journal of Geophysical Research: Atmospheres*, **122 (23)**, 12,653–12,671, doi:https://doi.org/10.1002/2017JD027543, URL https://agupubs.onlinelibrary.wiley.com/doi/abs/10.1002/2017JD027543, https://agupubs.onlinelibrary.wiley.com/doi/pdf/10.1002/2017JD027543.

Brown, M. E., and C. C. Funk, 2008: Food security under climate change. *Science*, **319 (5863)**, 580–581, doi:10.1126/science.1154102, URL https://www.science.org/doi/abs/10.1126/science.1154102, https://www.science.org/doi/pdf/10.1126/science.1154102.

Dee, D. P., and Coauthors, 2011: The era-interim reanalysis: configuration and performance of the data assimilation system. *Quarterly Journal of the Royal Meteorological Society*, **137 (656)**, 553–597, doi:https://doi.org/10.1002/qj.828, URL https://rmets.onlinelibrary.wiley.com/doi/abs/10.1002/qj.828, https://rmets.onlinelibrary.wiley.com/doi/pdf/10.1002/qj.828.

Deman, V. M. H., A. Koppa, W. Waegeman, D. A. MacLeod, M. Bliss Singer, and D. G. Miralles, 2022: Seasonal prediction of horn of africa long rains using machine learning: The pitfalls of preselecting correlated predictors. *Frontiers in Water*, **4**, doi:10.3389/frwa.2022.1053020, URL https://www.frontiersin.org/articles/10.3389/frwa.2022.1053020.

Drumond, A., R. Nieto, L. Gimeno, and T. Ambrizzi, 2008: A lagrangian identification of major sources of moisture over central brazil and la plata basin. *Journal of Geophysical Research: Atmospheres*, **113 (D14)**, doi:https://doi.org/10.1029/2007JD009547,

URL https://agupubs.onlinelibrary.wiley.com/doi/abs/10.1029/2007JD009547, https://agupubs.onlinelibrary.wiley.com/doi/pdf/10.1029/2007JD009547.

Dyer, E., and R. Washington, 2021: Kenyan long rains: A subseasonal approach to process-based diagnostics. *Journal of Climate*, **34 (9)**, 3311 – 3326, doi:10.1175/JCLI-D-19-0914.1, URL https://journals.ametsoc.org/view/journals/clim/34/9/JCLI-D-19-0914.1.xml.

Dyer, E. L. E., D. B. A. Jones, J. Nusbaumer, H. Li, O. Collins, G. Vettoretti, and D. Noone, 2017: Congo basin precipitation: Assessing seasonality, regional interactions, and sources of moisture. *Journal of Geophysical Research: Atmospheres*, **122 (13)**, 6882–6898, doi:https://doi.org/10.1002/2016JD026240, URL https://agupubs.onlinelibrary.wiley.com/doi/abs/10.1002/2016JD026240, https://agupubs.onlinelibrary.wiley.com/doi/pdf/10.1002/2016JD026240.

Emanuel, K. A., 1991: A scheme for representing cumulus convection in large-scale models. *Journal of Atmospheric Sciences*, **48 (21)**, 2313 – 2329, doi:10.1175/1520-0469(1991)048<2313:ASFRCC>2.0.CO;2, URL https://journals.ametsoc.org/view/journals/atsc/48/21/1520-0469_1991_048_2313_asfrcc_2_0_co_2.xml.

FEWSNET, 2022: Immediate global action required to prevent famine in the horn of africa. URL https://fews.net/sites/default/files/Joint\%20Alert\%20on\%202023\%20MAM\%20Rains\%20Final_0.pdf.

Findell, K. L., P. W. Keys, R. J. van der Ent, B. R. Lintner, A. Berg, and J. P. Krasting, 2019: Rising temperatures increase importance of oceanic evaporation as a source for continental precipitation. *Journal of Climate*, **32 (22)**, 7713 – 7726, doi:10.1175/JCLI-D-19-0145.1, URL https://journals.ametsoc.org/view/journals/clim/32/22/jcli-d-19-0145.1.xml.

Fremme, A., and H. Sodemann, 2019: The role of land and ocean evaporation on the variability of precipitation in the yangtze river valley. *Hydrology and Earth System Sciences*, **23 (6)**, 2525–2540, doi:10.5194/hess-23-2525-2019, URL https://hess.copernicus.org/articles/23/2525/2019/.

Funk, C., and Coauthors, 2018: Examining the role of unusually warm indo-pacific sea-surface temperatures in recent african droughts. *Quarterly Journal of the Royal Meteorological Society*,

537 **144 (S1)**, 360–383, doi:https://doi.org/10.1002/qj.3266, URL https://rmets.onlinelibrary.wiley.
538 com/doi/abs/10.1002/qj.3266, https://rmets.onlinelibrary.wiley.com/doi/pdf/10.1002/qj.3266.

539 Funk, C., and Coauthors, 2019: Recognizing the famine early warning systems network:
540 Over 30 years of drought early warning science advances and partnerships promoting global
541 food security. *Bulletin of the American Meteorological Society*, **100 (6)**, 1011 – 1027,
542 doi:10.1175/BAMS-D-17-0233.1, URL https://journals.ametsoc.org/view/journals/bams/100/
543 6/bams-d-17-0233.1.xml.

544 Funk, C. C., A. Hoell, S. Shukla, G. J. Husak, and J. Michaelsen, 2016: The east african monsoon
545 system: Seasonal climatologies and recent variations: Chapter 10. *The Monsoons and Climate*
546 *Change*, Springer, Cham, 163–185.

547 García-Herrera, R., and Coauthors, 2019: The european 2016/17 drought. *Journal of Climate*,
548 **32 (11)**, 3169 – 3187, doi:10.1175/JCLI-D-18-0331.1, URL https://journals.ametsoc.org/view/
549 journals/clim/32/11/jcli-d-18-0331.1.xml.

550 Gimeno, L., A. Drumond, R. Nieto, R. M. Trigo, and A. Stohl, 2010: On the ori-
551 gin of continental precipitation. *Geophysical Research Letters*, **37 (13)**, doi:https://doi.
552 org/10.1029/2010GL043712, URL https://agupubs.onlinelibrary.wiley.com/doi/abs/10.1029/
553 2010GL043712, https://agupubs.onlinelibrary.wiley.com/doi/pdf/10.1029/2010GL043712.

554 Gimeno, L., R. Nieto, and R. Sorí, 2020: The growing importance of oceanic moisture sources
555 for continental precipitation. *npj Climate and Atmospheric Science*, **3 (1)**, 27, doi:10.1038/
556 s41612-020-00133-y, URL https://doi.org/10.1038/s41612-020-00133-y.

557 Gong, C., and E. Eltahir, 1996: Sources of moisture for rainfall in west africa. *Water Re-*
558 *sources Research*, **32 (10)**, 3115–3121, doi:https://doi.org/10.1029/96WR01940, URL https:
559 //agupubs.onlinelibrary.wiley.com/doi/abs/10.1029/96WR01940, https://agupubs.onlinelibrary.
560 wiley.com/doi/pdf/10.1029/96WR01940.

561 Haile, G. G., and Coauthors, 2020: Projected impacts of climate change on drought
562 patterns over east africa. *Earth's Future*, **8 (7)**, e2020EF001 502, doi:https://doi.
563 org/10.1029/2020EF001502, URL https://agupubs.onlinelibrary.wiley.com/doi/abs/10.1029/

2020EF001502, e2020EF001502 2020EF001502, https://agupubs.onlinelibrary.wiley.com/doi/pdf/10.1029/2020EF001502.

Herrera-Estrada, J. E., J. A. Martinez, F. Dominguez, K. L. Findell, E. F. Wood, and J. Sheffield, 2019: Reduced moisture transport linked to drought propagation across north america. *Geophysical Research Letters*, **46 (10)**, 5243–5253, doi:https://doi.org/10.1029/2019GL082475, URL https://agupubs.onlinelibrary.wiley.com/doi/abs/10.1029/2019GL082475, https://agupubs.onlinelibrary.wiley.com/doi/pdf/10.1029/2019GL082475.

Hersbach, H., and Coauthors, 2020: The era5 global reanalysis. *Quarterly Journal of the Royal Meteorological Society*, **146 (730)**, 1999–2049, doi:https://doi.org/10.1002/qj.3803, URL https://rmets.onlinelibrary.wiley.com/doi/abs/10.1002/qj.3803, https://rmets.onlinelibrary.wiley.com/doi/pdf/10.1002/qj.3803.

Holgate, C. M., A. I. J. M. Van Dijk, J. P. Evans, and A. J. Pitman, 2020: Local and remote drivers of southeast australian drought. *Geophysical Research Letters*, **47 (18)**, e2020GL090 238, doi:https://doi.org/10.1029/2020GL090238, URL https://agupubs.onlinelibrary.wiley.com/doi/abs/10.1029/2020GL090238, e2020GL090238 2020GL090238, https://agupubs.onlinelibrary.wiley.com/doi/pdf/10.1029/2020GL090238.

Hsiang, S. M., M. Burke, and E. Miguel, 2013: Quantifying the influence of climate on human conflict. *Science*, **341 (6151)**, 1235 367, doi:10.1126/science.1235367, URL https://www.science.org/doi/abs/10.1126/science.1235367, https://www.science.org/doi/pdf/10.1126/science.1235367.

Huffman, G. J., D. T. Bolvin, D. Braithwaite, K. Hsu, R. Joyce, P. Xie, and S.-H. Yoo, 2015: Nasa global precipitation measurement (gpm) integrated multi-satellite retrievals for gpm (imerg). *Algorithm Theoretical Basis Document (ATBD) Version*, **4 (26)**.

Insua-Costa, D., M. Senande-Rivera, M. C. Llasat, and G. Miguez-Macho, 2022: A global perspective on western mediterranean precipitation extremes. *npj Climate and Atmospheric Science*, **5 (1)**, 9, doi:10.1038/s41612-022-00234-w, URL https://doi.org/10.1038/s41612-022-00234-w.

Keune, J., and D. G. Miralles, 2019: A precipitation recycling network to assess freshwater vulnerability: Challenging the watershed convention. *Water Resources Research*, **55 (11)**,

9947–9961, doi:https://doi.org/10.1029/2019WR025310, URL https://agupubs.onlinelibrary.wiley.com/doi/abs/10.1029/2019WR025310, https://agupubs.onlinelibrary.wiley.com/doi/pdf/10.1029/2019WR025310.

Keune, J., D. L. Schumacher, and D. G. Miralles, 2022: A unified framework to estimate the origins of atmospheric moisture and heat using lagrangian models. *Geoscientific Model Development*, **15 (5)**, 1875–1898, doi:10.5194/gmd-15-1875-2022, URL https://gmd.copernicus.org/articles/15/1875/2022/.

Liebmann, B., and Coauthors, 2014: Understanding recent eastern horn of africa rainfall variability and change. *Journal of Climate*, **27 (23)**, 8630 – 8645, doi:10.1175/JCLI-D-13-00714.1, URL https://journals.ametsoc.org/view/journals/clim/27/23/jcli-d-13-00714.1.xml.

MacLeod, D., 2019: Seasonal forecasts of the east african long rains: insight from atmospheric relaxation experiments. *Climate Dynamics*, **53 (7)**, 4505–4520, doi:10.1007/s00382-019-04800-6, URL https://doi.org/10.1007/s00382-019-04800-6.

MacLeod, D., R. Graham, C. O'Reilly, G. Otieno, and M. Todd, 2021: Causal pathways linking different flavours of enso with the greater horn of africa short rains. *Atmospheric Science Letters*, **22 (2)**, e1015, doi:https://doi.org/10.1002/asl.1015, URL https://rmets.onlinelibrary.wiley.com/doi/abs/10.1002/asl.1015, https://rmets.onlinelibrary.wiley.com/doi/pdf/10.1002/asl.1015.

Manatsa, D., and S. K. Behera, 2013: On the epochal strengthening in the relationship between rainfall of east africa and iod. *Journal of Climate*, **26 (15)**, 5655 – 5673, doi:10.1175/JCLI-D-12-00568.1, URL https://journals.ametsoc.org/view/journals/clim/26/15/jcli-d-12-00568.1.xml.

Martens, B., and Coauthors, 2017: Gleam v3: satellite-based land evaporation and root-zone soil moisture. *Geoscientific Model Development*, **10 (5)**, 1903–1925, doi:10.5194/gmd-10-1903-2017, URL https://gmd.copernicus.org/articles/10/1903/2017/.

Maystadt, J.-F., and O. Ecker, 2014: Extreme weather and civil war: Does drought fuel conflict in somalia through livestock price shocks? *American Journal of Agricultural Economics*, **96 (4)**, 1157–1182, doi:https://doi.org/10.1093/ajae/aau010, URL https://onlinelibrary.wiley.com/doi/abs/10.1093/ajae/aau010, https://onlinelibrary.wiley.com/doi/pdf/10.1093/ajae/aau010.

McPhaden, M. J., 1999: Genesis and evolution of the 1997-98 el nino. *Science*, **283 (5404)**, 950–954, doi:10.1126/science.283.5404.950, URL https://www.science.org/doi/abs/10.1126/science.283.5404.950.

Miralles, D. G., T. R. H. Holmes, R. A. M. De Jeu, J. H. Gash, A. G. C. A. Meesters, and A. J. Dolman, 2011: Global land-surface evaporation estimated from satellite-based observations. *Hydrology and Earth System Sciences*, **15 (2)**, 453–469, doi:10.5194/hess-15-453-2011, URL https://hess.copernicus.org/articles/15/453/2011/.

Miralles, D. G., and Coauthors, 2016: Contribution of water-limited ecoregions to their own supply of rainfall. *Environmental Research Letters*, **11 (12)**, 124 007, doi:10.1088/1748-9326/11/12/124007, URL https://doi.org/10.1088/1748-9326/11/12/124007.

Munday, C., R. Washington, and N. Hart, 2021: African low-level jets and their importance for water vapor transport and rainfall. *Geophysical Research Letters*, **48 (1)**, e2020GL090 999, doi:https://doi.org/10.1029/2020GL090999, URL https://agupubs.onlinelibrary.wiley.com/doi/abs/10.1029/2020GL090999, e2020GL090999 2020GL090999, https://agupubs.onlinelibrary.wiley.com/doi/pdf/10.1029/2020GL090999.

Niang, C., A. M. Mancho, V. J. García-Garrido, E. Mohino, B. Rodriguez-Fonseca, and J. Curbelo, 2020: Transport pathways across the west african monsoon as revealed by lagrangian coherent structures. *Scientific Reports*, **10 (1)**, 12 543, doi:10.1038/s41598-020-69159-9, URL https://doi.org/10.1038/s41598-020-69159-9.

Nicholson, S. E., 2015: Long-term variability of the east african 'short rains' and its links to large-scale factors. *International Journal of Climatology*, **35 (13)**, 3979–3990, doi:https://doi.org/10.1002/joc.4259, URL https://rmets.onlinelibrary.wiley.com/doi/abs/10.1002/joc.4259, https://rmets.onlinelibrary.wiley.com/doi/pdf/10.1002/joc.4259.

Nicholson, S. E., A. H. Fink, C. Funk, D. A. Klotter, and A. R. Satheesh, 2022: Meteorological causes of the catastrophic rains of october/november 2019 in equatorial africa. *Global and Planetary Change*, **208**, 103 687, doi:https://doi.org/10.1016/j.gloplacha.2021.103687, URL https://www.sciencedirect.com/science/article/pii/S0921818121002721.

Nieto, R., R. Castillo, A. Drumond, and L. Gimeno, 2014: A catalog of moisture sources for continental climatic regions. *Water Resources Research*, **50 (6)**, 5322–5328, doi:https://doi.org/10.1002/2013WR013901, URL https://agupubs.onlinelibrary.wiley.com/doi/abs/10.1002/2013WR013901, https://agupubs.onlinelibrary.wiley.com/doi/pdf/10.1002/2013WR013901.

Nieto, R., L. Gimeno, and R. M. Trigo, 2006: A lagrangian identification of major sources of sahel moisture. *Geophysical Research Letters*, **33 (18)**, doi:https://doi.org/10.1029/2006GL027232, URL https://agupubs.onlinelibrary.wiley.com/doi/abs/10.1029/2006GL027232, https://agupubs.onlinelibrary.wiley.com/doi/pdf/10.1029/2006GL027232.

Pettitt, A. N., 1979: A non-parametric approach to the change-point problem. *Journal of the Royal Statistical Society. Series C (Applied Statistics)*, **28 (2)**, 126–135, URL http://www.jstor.org/stable/2346729.

Rapolaki, R. S., R. C. Blamey, J. C. Hermes, and C. J. C. Reason, 2020: Moisture sources associated with heavy rainfall over the limpopo river basin, southern africa. *Climate Dynamics*, **55 (5)**, 1473–1487, doi:10.1007/s00382-020-05336-w, URL https://doi.org/10.1007/s00382-020-05336-w.

Rowell, D. P., B. B. B. Booth, S. E. Nicholson, and P. Good, 2015: Reconciling past and future rainfall trends over east africa. *Journal of Climate*, **28 (24)**, 9768 – 9788, doi:10.1175/JCLI-D-15-0140.1, URL https://journals.ametsoc.org/view/journals/clim/28/24/jcli-d-15-0140.1.xml.

Rybski, D., and J. Neumann, 2011: *A Review on the Pettitt Test Pettitt-test*, 202–213. Springer Berlin Heidelberg, Berlin, Heidelberg, doi:10.1007/978-3-642-14863-7_10, URL https://doi.org/10.1007/978-3-642-14863-7_10.

Sahlu, D., S. A. Moges, E. I. Nikolopoulos, E. N. Anagnostou, and D. Hailu, 2017: Evaluation of high-resolution multisatellite and reanalysis rainfall products over east africa. *Adv. Meteorol.*, **2017**, 1–14.

Saji, N. H., B. N. Goswami, P. N. Vinayachandran, and T. Yamagata, 1999: A dipole mode in the tropical indian ocean. *Nature*, **401 (6751)**, 360–363, doi:10.1038/43854, URL https://doi.org/10.1038/43854.

Salih, A. A. M., Q. Zhang, and M. Tjernström, 2015: Lagrangian tracing of sahelian sudan moisture sources. *Journal of Geophysical Research: Atmospheres*, **120 (14)**, 6793–6808, doi:https://doi.org/10.1002/2015JD023238, URL https://agupubs.onlinelibrary.wiley.com/doi/abs/10.1002/2015JD023238, https://agupubs.onlinelibrary.wiley.com/doi/pdf/10.1002/2015JD023238.

Schumacher, D. L., J. Keune, P. Dirmeyer, and D. G. Miralles, 2022: Drought self-propagation in drylands due to land–atmosphere feedbacks. *Nature Geoscience*, **15 (4)**, 262–268, doi:10.1038/s41561-022-00912-7, URL https://doi.org/10.1038/s41561-022-00912-7.

Schumacher, D. L., J. Keune, C. C. van Heerwaarden, J. Vilà-Guerau de Arellano, A. J. Teuling, and D. G. Miralles, 2019: Amplification of mega-heatwaves through heat torrents fuelled by upwind drought. *Nature Geoscience*, **12 (9)**, 712–717, doi:10.1038/s41561-019-0431-6, URL https://doi.org/10.1038/s41561-019-0431-6.

Sodemann, H., 2020: Beyond turnover time: Constraining the lifetime distribution of water vapor from simple and complex approaches. *Journal of the Atmospheric Sciences*, **77 (2)**, 413 – 433, doi:10.1175/JAS-D-18-0336.1, URL https://journals.ametsoc.org/view/journals/atsc/77/2/jas-d-18-0336.1.xml.

Sodemann, H., V. Masson-Delmotte, C. Schwierz, B. M. Vinther, and H. Wernli, 2008: Interannual variability of greenland winter precipitation sources: 2. effects of north atlantic oscillation variability on stable isotopes in precipitation. *Journal of Geophysical Research: Atmospheres*, **113 (D12)**, doi:https://doi.org/10.1029/2007JD009416, URL https://agupubs.onlinelibrary.wiley.com/doi/abs/10.1029/2007JD009416, https://agupubs.onlinelibrary.wiley.com/doi/pdf/10.1029/2007JD009416.

Sorí, R., J. A. Marengo, R. Nieto, A. Drumond, and L. Gimeno, 2018: The atmospheric branch of the hydrological cycle over the negro and madeira river basins in the amazon region. *Water*, **10 (6)**, doi:10.3390/w10060738, URL https://www.mdpi.com/2073-4441/10/6/738.

Staal, A., I. Fetzer, L. Wang-Erlandsson, J. H. C. Bosmans, S. C. Dekker, E. H. van Nes, J. Rockström, and O. A. Tuinenburg, 2020: Hysteresis of tropical forests in the 21st century. *Nature Communications*, **11 (1)**, 4978, doi:10.1038/s41467-020-18728-7, URL https://doi.org/10.1038/s41467-020-18728-7.

Stohl, A., C. Forster, A. Frank, P. Seibert, and G. Wotawa, 2005: Technical note: The lagrangian particle dispersion model flexpart version 6.2. *Atmospheric Chemistry and Physics*, **5 (9)**, 2461–2474, doi:10.5194/acp-5-2461-2005, URL https://acp.copernicus.org/articles/5/2461/2005/.

Te Wierik, S. A., J. Keune, D. G. Miralles, J. Gupta, Y. A. Artzy-Randrup, L. Gimeno, R. Nieto, and L. H. Cammeraat, 2022: The contribution of transpiration to precipitation over african watersheds. *Water Resources Research*, **58 (11)**, e2021WR031 721, doi: https://doi.org/10.1029/2021WR031721, URL https://agupubs.onlinelibrary.wiley.com/doi/abs/10.1029/2021WR031721, e2021WR031721 2021WR031721, https://agupubs.onlinelibrary.wiley.com/doi/pdf/10.1029/2021WR031721.

Tierney, J. E., C. C. Ummenhofer, and P. B. deMenocal, 2015: Past and future rainfall in the horn of africa. *Science Advances*, **1 (9)**, e1500 682, doi:10.1126/sciadv.1500682, URL https://www.science.org/doi/abs/10.1126/sciadv.1500682, https://www.science.org/doi/pdf/10.1126/sciadv.1500682.

Tuinenburg, O. A., J. J. E. Theeuwen, and A. Staal, 2020: High-resolution global atmospheric moisture connections from evaporation to precipitation. *Earth System Science Data*, **12 (4)**, 3177–3188, doi:10.5194/essd-12-3177-2020, URL https://essd.copernicus.org/articles/12/3177/2020/.

van der Ent, R. J., and H. H. G. Savenije, 2013: Oceanic sources of continental precipitation and the correlation with sea surface temperature. *Water Resources Research*, **49 (7)**, 3993–4004, doi:https://doi.org/10.1002/wrcr.20296, URL https://agupubs.onlinelibrary.wiley.com/doi/abs/10.1002/wrcr.20296, https://agupubs.onlinelibrary.wiley.com/doi/pdf/10.1002/wrcr.20296.

van der Ent, R. J., H. H. G. Savenije, B. Schaefli, and S. C. Steele-Dunne, 2010: Origin and fate of atmospheric moisture over continents. *Water Resources Research*, **46 (9)**, doi:https://doi.org/10.1029/2010WR009127, URL https://agupubs.onlinelibrary.wiley.com/doi/abs/10.1029/2010WR009127, https://agupubs.onlinelibrary.wiley.com/doi/pdf/10.1029/2010WR009127.

Vellinga, M., and S. F. Milton, 2018: Drivers of interannual variability of the east african "long rains". *Quarterly Journal of the Royal Meteorological Society*, **144 (712)**, 861–876, doi:https://doi.org/10.1002/qj.3263, URL https://rmets.onlinelibrary.wiley.com/doi/abs/10.1002/qj.3263, https://rmets.onlinelibrary.wiley.com/doi/pdf/10.1002/qj.3263.

Wainwright, C. M., J. H. Marsham, R. J. Keane, D. P. Rowell, D. L. Finney, E. Black, and R. P. Allan, 2019: 'eastern african paradox' rainfall decline due to shorter not less intense long rains. *npj Climate and Atmospheric Science*, **2 (1)**, 34, doi:10.1038/s41612-019-0091-7, URL https://doi.org/10.1038/s41612-019-0091-7.

Walker, D. P., J. H. Marsham, C. E. Birch, A. A. Scaife, and D. L. Finney, 2020: Common mechanism for interannual and decadal variability in the east african long rains. *Geophysical Research Letters*, **47 (22)**, e2020GL089 182, doi:https://doi.org/10.1029/2020GL089182, URL https://agupubs.onlinelibrary.wiley.com/doi/abs/10.1029/2020GL089182, e2020GL089182 10.1029/2020GL089182, https://agupubs.onlinelibrary.wiley.com/doi/pdf/10.1029/2020GL089182.

Williams, A. P., and C. Funk, 2011: A westward extension of the warm pool leads to a westward extension of the walker circulation, drying eastern africa. *Climate Dynamics*, **37 (11)**, 2417–2435, doi:10.1007/s00382-010-0984-y, URL https://doi.org/10.1007/s00382-010-0984-y.

Yu, L., and R. A. Weller, 2007: Objectively analyzed air–sea heat fluxes for the global ice-free oceans (1981–2005). *Bulletin of the American Meteorological Society*, **88 (4)**, 527 – 540, doi:10.1175/BAMS-88-4-527, URL https://journals.ametsoc.org/view/journals/bams/88/4/bams-88-4-527.xml.

Zemp, D. C., and Coauthors, 2017: Self-amplified amazon forest loss due to vegetation-atmosphere feedbacks. *Nature Communications*, **8 (1)**, 14 681, doi:10.1038/ncomms14681, URL https://doi.org/10.1038/ncomms14681.

FIG. 1. **a**. Horn of Africa drylands (HAD). **b**. Average annual cycle of rainfall in the HAD region, averaged over 1980–2016, indicating the two most important seasons, i.e., the long rain season from March–May (blue) and the short rain season from October–December (green). **c** and **d**. Time series of rainfall anomalies during the long and short rains respectively over the HAD region from 1980–2016. Dashed lines represent the change point based on Pettitt's test. The red lines represent the mean precipitation anomalies for the time periods before and after the change point. The rainfall during the short rains in 1997 was not considered in the calculation of the mean anomalies due to the exceptional nature of ENSO.

FIG. 2. **a** and **b**. Source regions of rainfall during long (a) and short rains (b), averaged over the time period 1980–2016. The source region represents the smallest region contributing 95% of the climatological mean rainfall during the long and short rains. The red outline corresponds to the smallest source region contributing 50% of the rainfall for each season. **c** and **d**. Long-term mean in integrated water vapour transport (IVT) during the long (c) and short (d) rains. The arrows represent the corresponding prevailing wind directions.

FIG. 3. Source regions of rainfall for **a**. March, **b**. April, **c**. May, **d**. October, **e**. November, **f**. December, calculated over the time period 1980–2016. The arrows represent wind magnitude and direction at 850 hPa.

FIG. 4. Time series of moisture contributions to rainfall from local recycling, external land, and ocean sources during the long (**a**) and short (**b**) rains respectively. The horizontal bars at the top of the plots represent the relative percentage contribution from different sources before and after the change point.

FIG. 5. **a** and **b**. Source regions of rainfall over the Horn of Africa drylands during the long rains, averaged over anomalously wet and dry years, respectively. The arrows represent wind speed and direction at 850 hPa. **c** and **d**. Anomalies of source region contributions to rainfall for the cases shown in **a** and **b**, respectively.

FIG. 6. **a**, **b**, and **c**. Source regions of evaporation contributing to rainfall over the Horn of Africa drylands during the short rains, averaged over anomalously wet, dry years and the exceptional El Niño and IOD year of 1997, respectively. Arrows represent wind speed and direction at 850 hPa. **d**, **e** and **f**. Anomalies of evaporation from the source region for the cases shown in **a**, **b**, and **c**.

FIG. 7. Time series of normalized anomalies of total evaporation from the source region (E (Source)) compared to precipitation in the HAD region (P (sink)) for the long (**a**) and short (**b**) rains. E (source) is estimated by weighing evaporation from each grid cell in the source region by their relative contribution to rainfall in the HAD region.

Figure 1.

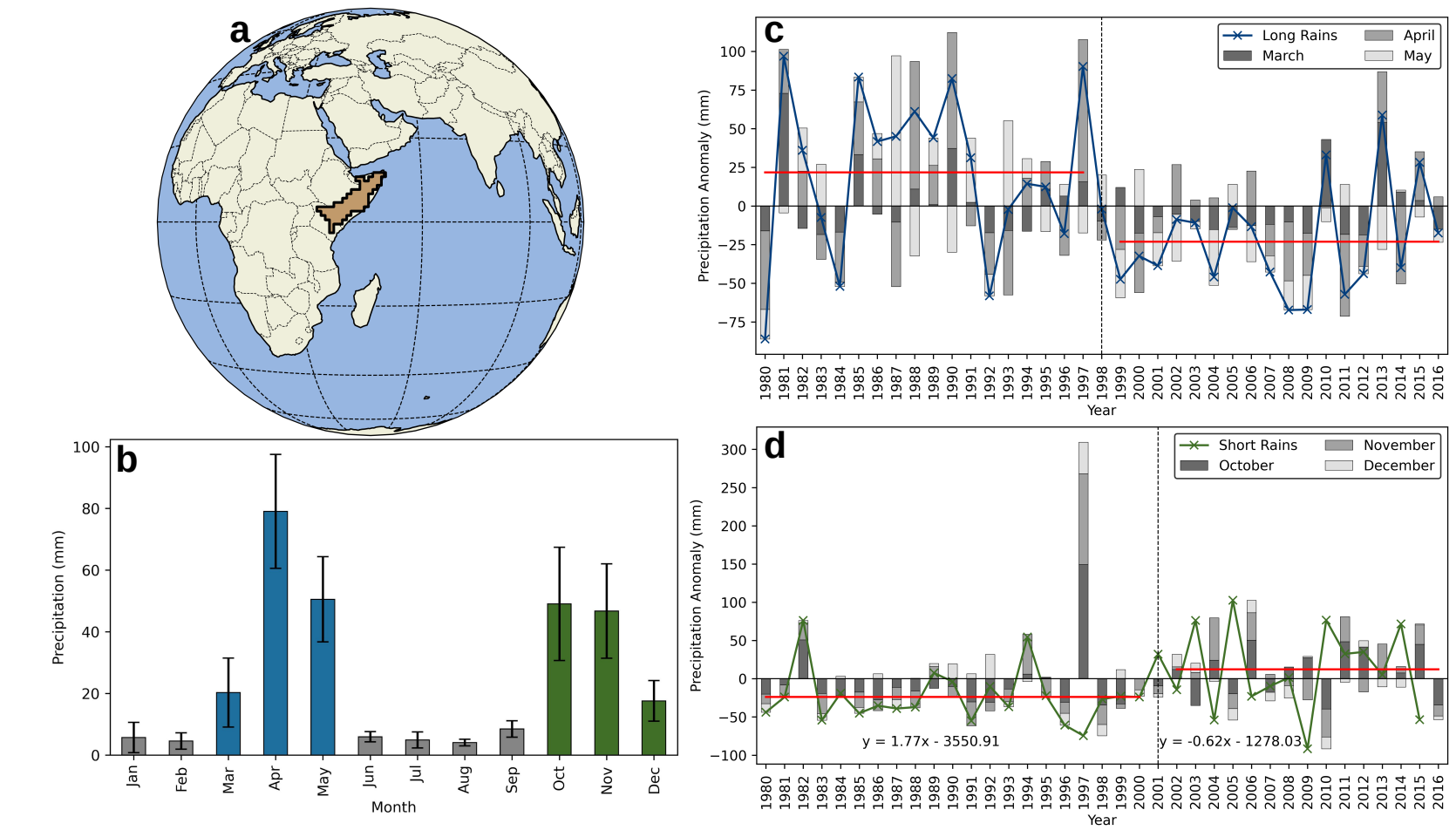
a
b
Precipitation (mm)
Month
Jan
Feb
Mar
Apr
May
Jun
Jul
Aug
Sep
Oct
Nov
Dec
c
Long Rains
March
April
May
Precipitation Anomaly (mm)
Year
d
Short Rains
October
November
December
y = 1.77x - 3550.91
y = -0.62x - 1278.03
Precipitation Anomaly (mm)
Year

Figure 2.

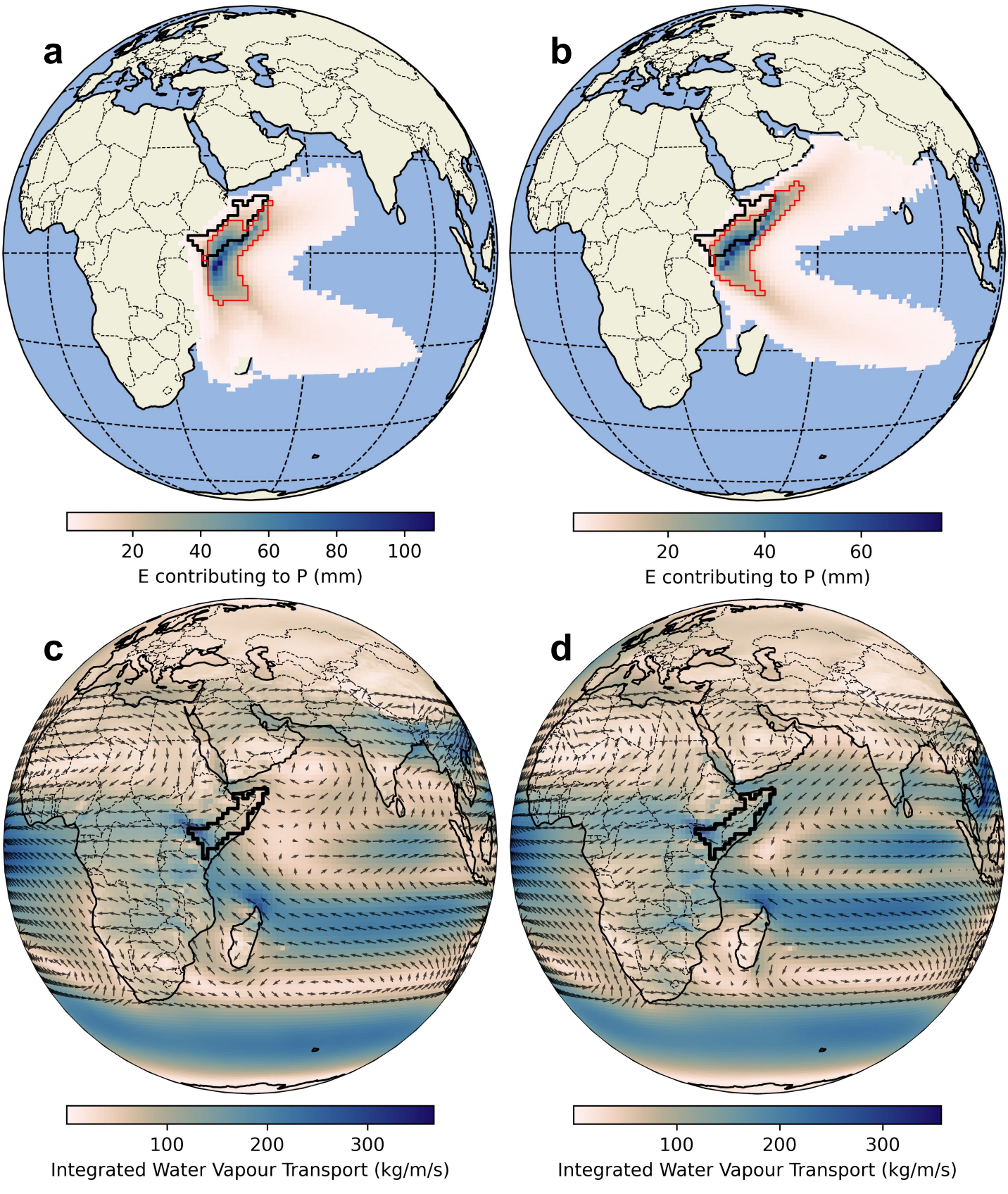
a
b
20
40
60
80
100
E contributing to P (mm)
20
40
60
E contributing to P (mm)
c
d
100
200
300
Integrated Water Vapour Transport (kg/m/s)
100
200
300
Integrated Water Vapour Transport (kg/m/s)

Figure 3.

a

6.0 m/s

5 10 15

E contributing to P (mm/month)

b

6.0 m/s

10 20 30 40 50

E contributing to P (mm/month)

c

6.0 m/s

10 20 30

E contributing to P (mm/month)

d

6.0 m/s

10 20 30

E contributing to P (mm/month)

e

6.0 m/s

10 20 30

E contributing to P (mm/month)

f

6.0 m/s

2.5 5.0 7.5 10.0 12.5

E contributing to P (mm/month)

Figure 4.

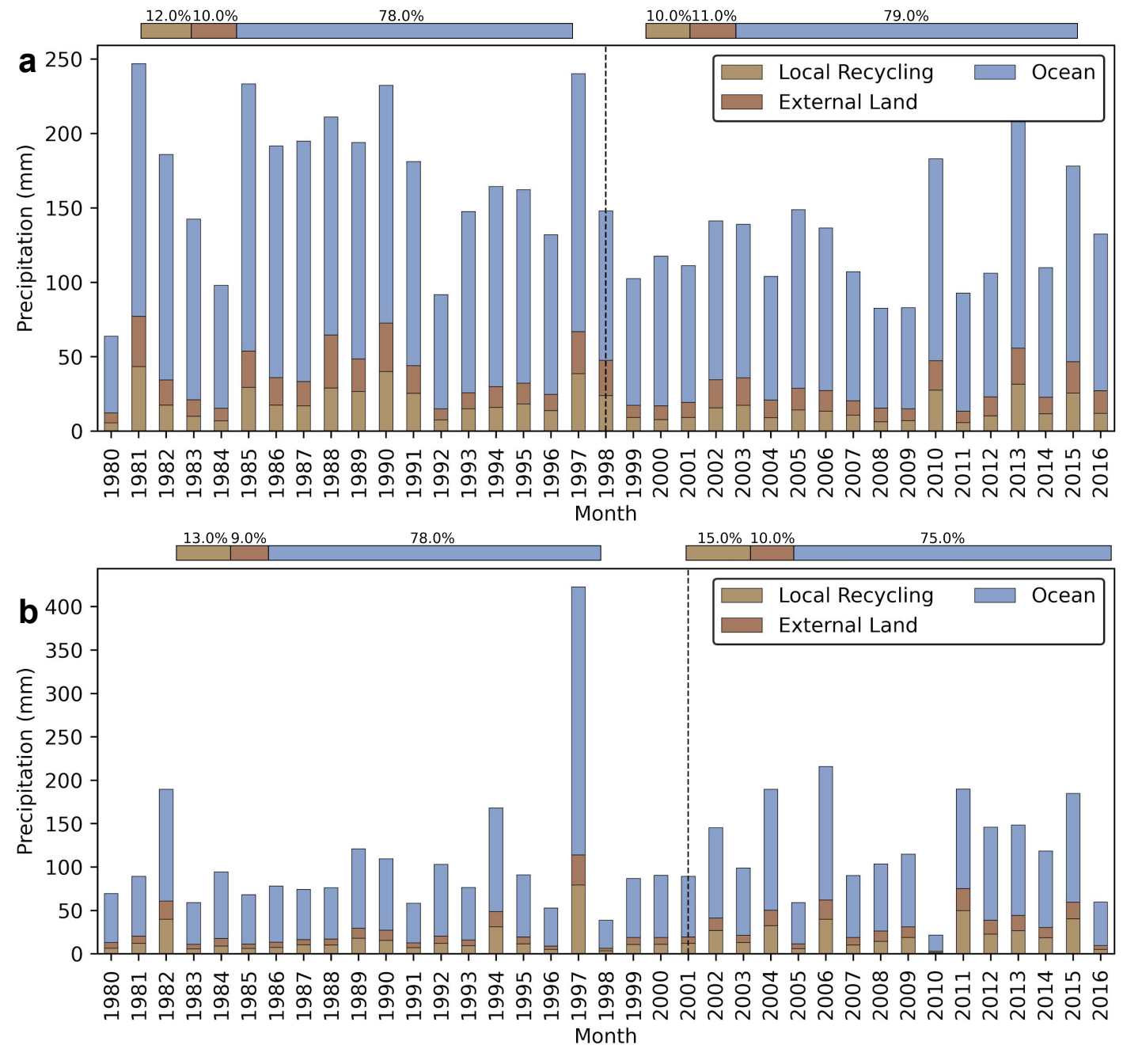
a
12.0%
10.0%
78.0%
10.0%
11.0%
79.0%
Local Recycling
External Land
Ocean
Precipitation (mm)
Month
b
13.0%
9.0%
78.0%
15.0%
10.0%
75.0%
Local Recycling
External Land
Ocean
Precipitation (mm)
Month

Figure 5.

a

6.0 m/s

50 100 150

E contributing to P (mm)

b

6.0 m/s

20 40 60

E contributing to P (mm)

c

0 10 20 30 40 50 60 70

E contributing to P (mm)

d

−70 −60 −50 −40 −30 −20 −10 0

E contributing to P (mm)

Figure 6.

a

6.0 m/s

20 40 60 80 100

E contributing to P (mm)

b

6.0 m/s

10 20 30 40

E contributing to P (mm)

c

6.0 m/s

50 100 150

E contributing to P (mm)

d

0 10 20 30 40 50 60 70

E contributing to P (mm)

e

−70 −60 −50 −40 −30 −20 −10 0

E contributing to P (mm)

f

0 20 40 60 80 100 120 140

E contributing to P (mm)

Figure 7.

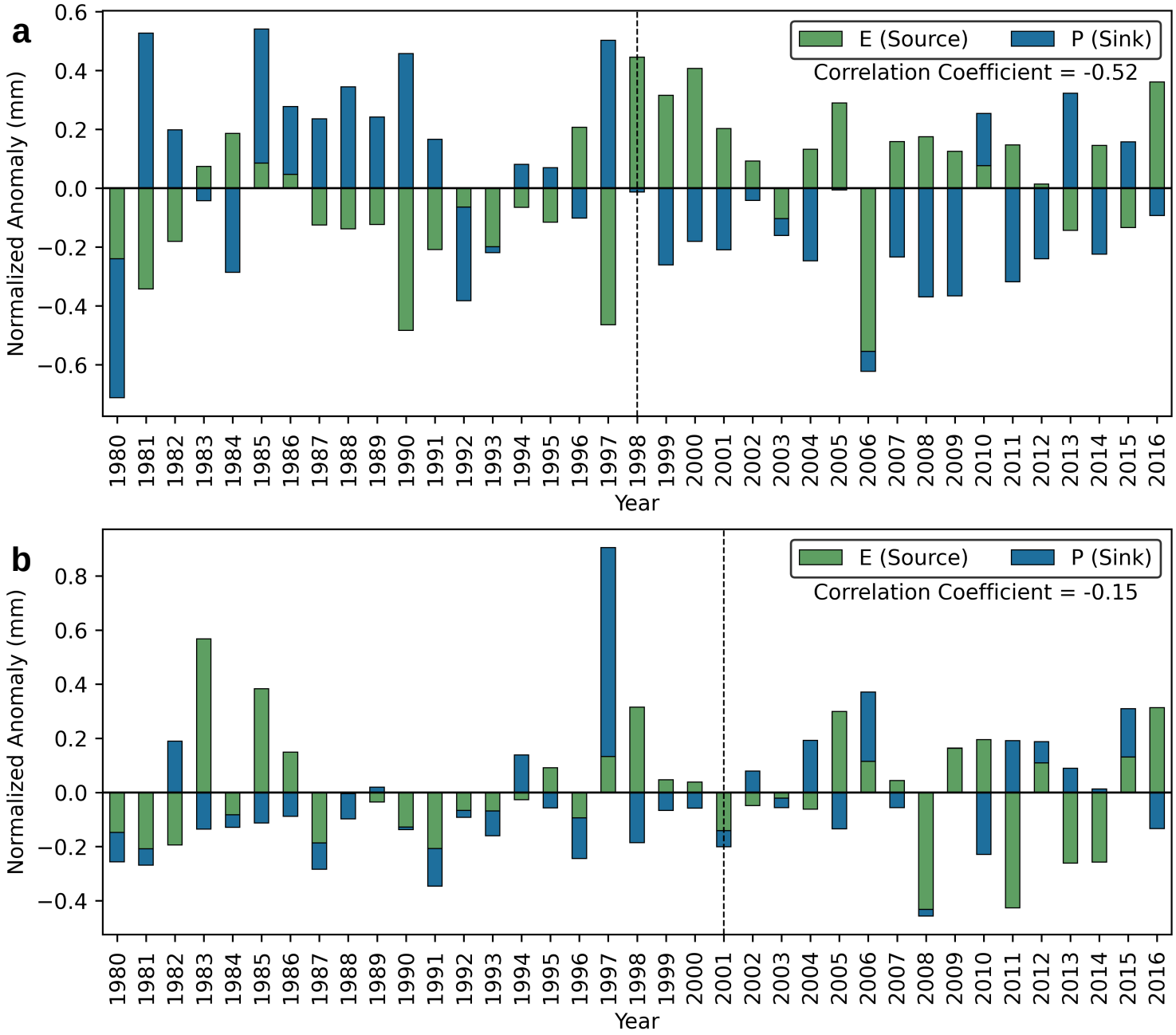
a
E (Source)
P (Sink)
Correlation Coefficient = -0.52
Normalized Anomaly (mm)
0.6
0.4
0.2
0.0
−0.2
−0.4
−0.6
1980 1981 1982 1983 1984 1985 1986 1987 1988 1989 1990 1991 1992 1993 1994 1995 1996 1997 1998 1999 2000 2001 2002 2003 2004 2005 2006 2007 2008 2009 2010 2011 2012 2013 2014 2015 2016
Year
b
E (Source)
P (Sink)
Correlation Coefficient = -0.15
Normalized Anomaly (mm)
0.8
0.6
0.4
0.2
0.0
−0.2
−0.4
1980 1981 1982 1983 1984 1985 1986 1987 1988 1989 1990 1991 1992 1993 1994 1995 1996 1997 1998 1999 2000 2001 2002 2003 2004 2005 2006 2007 2008 2009 2010 2011 2012 2013 2014 2015 2016
Year